RESEARCH ON THE SHEAR ANGLE THEORY BASED ON THE INTERNAL FRICTION IN HIGH-SPEED CUTTING OF HIGH-ENTROPY ALLOY FeCoNiCrAl

Y. J. Tang, Z. Xie, D. C. Xu,[1]   UDC 539.4
and H. Feng

High-entropy alloys are typically emerging and difficult-to-cut multi-element alloys with high hardness, high strength and good fatigue performance and are considered to have good application prospects, but their processability remains to be studied. High-speed cutting, as a mature rough processing for hard-to-machine alloys, is characterized by serrated chips and is attributed to the shear, compression and internal friction within the primary deformation zone. However, in conventional shear angle theories, the effect of internal friction is often ignored, resulting in unstable accuracy when these theories are applied to high-speed cutting. Improving the existing shear angle theories will elaborate the balance between deformation and friction in high-speed cutting more clearly, which has certain instructiveness to engineering applications. Thus, an improved shear angle model considering internal friction is combined herein with orthogonal high-speed cutting experiments on the high-entropy alloy FeCoNiCrAl to obtain the cutting performance of the material. After modification, the scope of application of shear angle theories was expanded from low-speed cutting to high-speed cutting. The internal friction angle is mainly affected by the cutting speed as well as the thermal conductivity of materials.

Keywords: high-entropy alloys, high-speed cutting, internal friction, serrated chip.

Introduction. Newly developed high-entropy alloys (HEAs) are composed of at least five main elements, where each component comprises 5–35% of the concentration of the alloy [1]. Miracle and Senkov divided high-entropy alloys into seven categories according to their compositions. Among them, the 3d transition metal is the most widely studied high-entropy alloy system, which usually includes four of the following nine elements: Al, Co, Cr, Cu, Fe, Mn, Ni, Ti, and V. In addition, high-temperature nickel-based alloys can be considered medium/high entropy alloys composed of three to five elements in Ni, Cr, Co, Fe, and Mo [2]. The similarity in composition makes the FeCoNiCrAl 3d transition alloy an extension of high-temperature alloys and a kind of refractory alloy. In terms of application, these HEAs are widely used in high-speed cutting tools and marine and aerospace equipment owing to their excellent

properties, such as high hardness and strength, corrosion resistance and special electrical and magnetic properties [2, 3]. There have been HEA studies on ingredient proportions [4], preparation technology [5] and dynamic mechanical properties [6], but very little research regarding the cutting properties of HEAs has been published.

From the studies of Li et al. [7] and Su et al. [8], high-speed cutting is a mature rough machining method that is commonly used in processing difficult-to-cut materials, and thus, this cutting method is also adopted for HEA machining in this study. It is difficult to distinguish low-speed cutting from high-speed cutting only by cutting velocity because the critical speed of high-speed cutting varies with materials, but the phenomenon that ribbon chips turn into serrated chips can be taken as a reliable sign of high-speed cutting [9]. The serrated chip is of great significance in revealing the mechanism of high-speed cutting because it embodies the two basic cutting behaviors of deformation and friction.

Yang et al. [10] characterized serrated chips from the perspective of geometry and mechanics, and a number of models have been proposed to investigate the formation mechanism of serrated chips. For example, Ke et al. [11] proposed an orthogonal high-speed cutting model to study the relationship between the shear slip characteristics, the cutting zone and the cutting parameters of serrated chips. Furthermore, a theoretical model was constructed to directly calculate the shear angle using the chip geometric parameters without being restricted by the cutting speed [12]. Fu et al. [13] established a modified constitutive model of high-speed cutting of rolled sheets of aviation aluminum alloy 7050-T7451 that considered anisotropy through experiments such as SHPB. Ullah et al. [14] proposed a numerical method for the formation of high-speed milling sawtooth chips for Ti-6Al-4V alloys that are different from turning, which helps to better understand the formation process of sawtooth chips in high-speed milling. The finite element method (FEM) has been widely used in mechanism research because of its rationality and low consumption. Jomaa et al. [15] found by combining an orthogonal cutting experiment and FEM that the cause of serrated chip formation on the AA7075-T651 material is shear strain localization from the tool tip to the free surface of the workpiece, while for Inconel 718, based on the study of Wang et al. [16], serrated chip formation is caused by plastic deformation and ductile fracture. Therefore, it is inferred that chip formation can be affected by material mechanical properties. By using three numerical formulas of LAG, ALE and CEL, Zhang et al. [17] established a finite element model of the orthogonal cutting process of A2024-T351 aluminum alloy and Ti6Al4V titanium alloy and deeply studied the mechanism of chip segmentation.

In addition to the influence within the primary deformation zone, serrated chips are also greatly affected by external friction (tool-chip friction), categorized as sliding friction, sticking-sliding friction and sticking friction according to the contact form. An arbitrary Lagrangian–Eulerian model [18] and a chip formation model [19] described the thermomechanical interactions along the tool-chip interface, where the latter research mainly focused on the sticking friction. Another model developed by Hao et al. [20] divided the external friction into three stages, wherein the sticking-sliding friction model was applicable to the peak friction between two materials' surfaces in the first stage, but the increasing wear debris present in the subsequent two stages formed a transfer layer to transmit the sliding friction. In addition to studying the regional length variation of three friction forms on the rake surface, Zhang et al. [21] also considered the thicknesses of the stagnation and shear flow layers that were presented in the viscous and

transition regions, respectively. Tu et al. [22] systematically studied the effects of different cutting speeds on the wear and failure mechanism of SiAlON ceramic tools during the dry cutting process of nickel-based superalloys. Duan et al. [23] presented a three-phase friction model based on whether the hard particles in Al/SiCp participated in external friction. The results showed that an increase in the particle volume fraction or particle size can lead to a reduction in the friction coefficient.

The equilibrium between shear deformation and external friction can be described by a classic theoretical system of shear angle, which has sufficient physical meaning under low-speed cutting, including models presented by Merchant and Eugene [24], Lee and Shaffer [25], Altintas [26], and Shaw [27], but loses its precision in high-speed cutting. It is believed that chip formation is caused by shear slip and tool-chip friction; however, the free surface of the serrated chip is not as smooth as the tool-ship squeezing interface, which means that there is not only shear deformation but also impact deformation in the primary deformation zone. (The uncut element entering the deformation zone has a relative velocity with the chip, leading the impact.) Li et al. [7] noted the compression within the primary deformation zone and proposed a model to obtain the relationship between the compression deformation characteristics and cutting parameters. Zhang et al. [28] found that in a series of ultra-precision machining right-angle orthogonal cutting tests, the shear angle evolved cyclically with the formation of chips in the sheet layer, and the cyclic shear angle model was obtained. Sui and Feng [29] attributed the plastic deformation of grains in the adiabatic shear zone to the extrusion effect of two adjacent sawtooth serrations. The existence of both extrusion and shear slip in the primary deformation zone leads to internal friction within the workpiece materials, which has not received enough attention as a mechanism behind a serrated chip.

Therefore, this paper modified the shear angle theory by considering the internal friction and a new formula for calculating the internal friction angle. To verify the improved model and obtain the cutting performance of the FeCoNiCrAl HEA, orthogonal high-speed cutting experiments were performed. In addition, the internal friction angles of the FeCoNiCrAl HEA, Al6061-T6 and Ti-6Al-4V were calculated by the modified formula and compared to counterparts of the classic theoretical system of shear angle to obtain the application scopes of the modified model and the new formula.

1. Theoretical Model. The Lee-Shaffer slip-line field theory gives the equilibrium relationship between the cutting deformation (via shear angle ϕ), external friction (via friction angle β) and internal friction (via internal friction angle β_{in}) during low-speed cutting and is expressed as

$$\phi + \beta - \gamma_0 = \pi/4, \qquad (1)$$

where γ_0 is the rake angle. The internal friction angle β_{in} is not included in Eq. (1) because the Lee–Shaffer theory assumes that internal friction occurring between materials with the same lattices should have a constant angle of 45°. This assumption does not account for the effects of the material inner structures or transformation of the material state via internal friction, however, and needs to be improved. Therefore, on the basis of serrated chips, a computational model for the internal friction angle is proposed in Fig. 1. The model expresses the complex mathematical relationships

between the parameters in a concise and clear geometric form. According to the work of Li et al., in addition to the shear stress (F_s), normal stress (N_s) introduced by the tool-chip extrusion also exists in the slip plane (represented by line AB in Fig. 1), and these two stresses eventually generate internal friction. In this model, deformations within slip plane AB can be divided into two stages. In the first stage, shear behavior occurs when the measured force F_s reaches the material's yield limit. After shearing, in the subsequent second stage, the material within the $AEFG$ and $ABCD$ regions begins to slide along plane AB with the effect of normal stress, and internal friction eventually occurs. The tool rake angle is known to be 0°, and the shear angle ϕ and friction angle β needed for the β_{in} calculation are given by

$$\phi = \arctan\left(\frac{a_c \cos\gamma_0}{\frac{H_1 + H_2}{2} - a_c \sin\gamma_0}\right), \tag{2}$$

$$\beta = \arctan\left(\frac{F_C \sin\gamma_0 + F_T \cos\gamma_0}{F_C \cos\gamma_0 - F_T \sin\gamma_0}\right), \tag{3}$$

where a_c is the cutting depth, H_1 and H_2 are the maximum and minimum serrated chip heights, respectively, and F_C and F_T are the cutting and thrust forces, respectively. Combining the definition of the internal friction angle and the geometric relationships in the theoretical model, the mechanism of internal friction deformation can be described using

$$\frac{1}{\tan\beta_{in}} = \frac{\sigma}{\tau_s} = \frac{N_s}{F_s} = \tan(\phi + \beta - \gamma_0), \tag{4}$$

where σ is the normal stress and τ_s is the shear strength. Finally, a formula for calculating the internal friction angle is deduced as

$$\beta_{in} = \pi/2 + \gamma_0 - \phi - \beta. \tag{5}$$
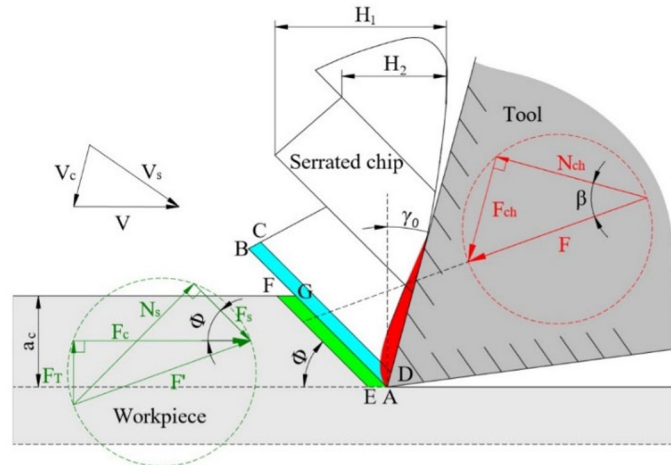

Fig. 1. Internal friction angle model based on serrated chips.

The internal friction coefficient, a parameter for indicating the internal friction, equals the ratio τ_s/σ_s. This coefficient is discussed in the classic theoretical system: the ratio equals 1/2 in the maximum shear stress yield

condition presented by Tresca, $\sqrt{3}/3$ in the specific energy of elastic deformation yield condition proposed by von Mises, and 1 in the shear angle theory deduced by Lee–Shaffer and Krystof. By this token, the values of the internal friction coefficient obtained by scholars vary significantly based on different theories. To compare the applicability and accuracy of these theories, a series of orthogonal high-speed cutting experiments of HEA FeCoNiCrAl were performed, and the corresponding shear angles and internal friction coefficients were calculated.

2. Orthogonal High-Speed Cutting Experiment. The orthogonal high-speed dry cutting experiment was carried out using a lathe (SMTCL CHK52) to explore the internal friction angle and cutting performances of HEA FeCoNiCrAl in this study. The experimental platform is shown in Fig. 2. We purchased the required experimental materials from a manufacturer specializing in HEA production. Workpieces were HEA sheet rings made of five main metals, including Fe (15%), Co (15%), Ni (37%), Cr (15%) and Al (18%), with abundant pits and precipitated metal particles distributed inside. The external diameter (120 mm) of the workpieces was determined by the cutting speed and cutting form, the inner diameter (12 mm) was matched with the workpiece fixture, and the workpiece thickness was the cutting width in the experiment. Details of the cutting parameters are listed in Table 1. During cutting, a tool (SECO-CCGW 09T304S-01020-LF(CBN010)) with a rake angle of 0° and a relief angle of 7° was inserted into a cutter bar (SECO-SCFCL 1212F09) and fed along the radial direction of the workpiece with the main cutting edge orthogonal to the direction of the cutting speed. To install a thermocouple (K-thermocouple) for temperature measurement, the head of the cutter bar was sunk 1 mm by grinding, and three temperature measuring holes with a diameter of 0.6 mm and depth of 3 mm were evenly machined in the base portion at the edge of the tool. Because the edge length of the tool was 9.7 mm, every edge was used three times without repetition to lower the tool cost. A cutter bar was mounted on a dynamometer (Kistler9119A1) to measure the cutting force. Finally, the geometry of the serrated chips was observed with field emission scanning electron microscopy (SEM; ZEISS MERLIN Compact).
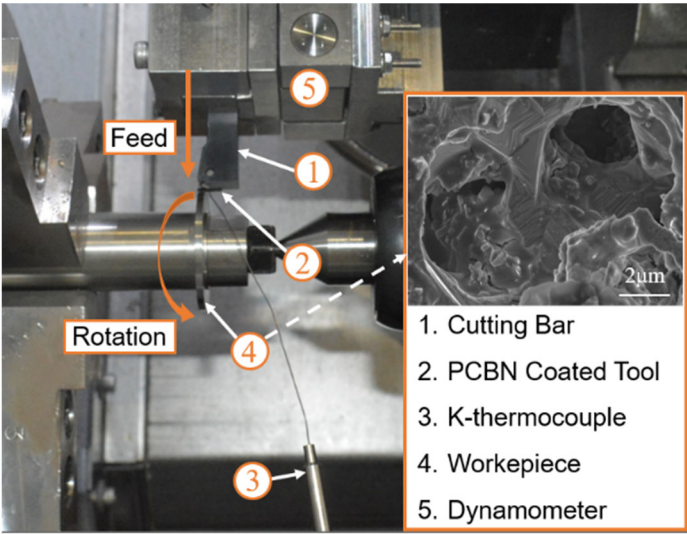

Fig. 2. Orthogonal high-speed dry cutting experimental setup.

TABLE 1. Experimental Parameters

Groups	Linear velocity, m/min	Feed rate, mm/rev	Cutting width, mm
1	50, 170, 300, 400	0.05	3.8
2	50, 170, 300, 400	0.1	3.8
3	50, 170, 300, 400	0.1	3.4
4	50, 170, 300, 400	0.1	2.5

3. Results and Discussion.

3.1. Cutting Force and Cutting Temperature. Considering the influence of the cutting-edge radius on cutting with a small feed rate ($f = 0.05$ mm/rev), only cutting forces with a feed rate of 0.1 mm/rev are analyzed in this study. Figure 3 shows that the cutting temperature increases with the cutting speed, and the highest local temperature measured at the temperature holes even rises to 568°C when the cutting speed reaches 400 m/min. As the cutting temperature rises, the thermal softening effect gradually exceeds the strain hardening effect, resulting in a decrease in the cutting force and thrust force, as shown in Fig. 4. In addition, it is also observed that cutting forces increase with the cutting width. According to the cutting experiment results, HEA FeCoNiCrAl produces local high temperature at high-speed cutting and is a difficult-to-machine alloy. To lower the cutting force, cutting settings with a high cutting speed, small feed rate and small cutting width are recommended.
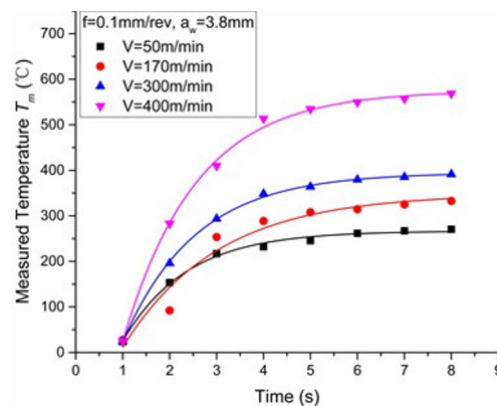

Fig. 3. Temperature measured at the thermocouple hole ($f = 0.1$ mm/rev, $a_w = 3.8$ mm, $V = 50$–400 m/min).

3.2. Characteristics of Serrated Chips. The shear angle and friction angle are important in serrated chip deformation because they represent the plastic deformation and external friction in the primary and secondary deformation zones, respectively. In addition, they are essential for calculating the internal friction angle in this study. Equation (2) shows that the shear angle is inversely proportional to the sum of the maximum and minimum serrated chip thicknesses, which are measured from the SEM micrographs of serrated chip geometries in Fig. 5. Figure 6 plots the maximum and minimum chip thicknesses as a function of cutting speed, where both thicknesses are observed to decrease with cutting speed. This signifies that the shear angle increases [via Eq. (2) and exhibited in Fig. 7], and plastic deformation subdues in the primary deformation zone during cutting, which is consistent with the experimental cutting force results. Note that the minimum chip thickness declines more rapidly, that is, the degree of serration becomes

more obvious. This phenomenon can result in rough surface quality and thus should be avoided. Figure 8 demonstrates that the external friction angle decreases as a function of cutting speed, according to Eq. (3).
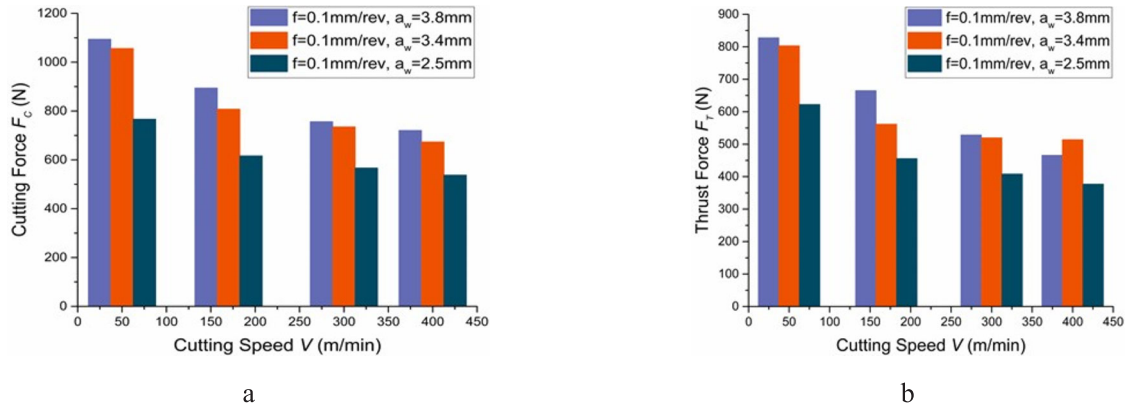

| a | b |

Fig. 4. (a) Cutting force and (b) thrust force as a function of cutting speed for various cutting widths.
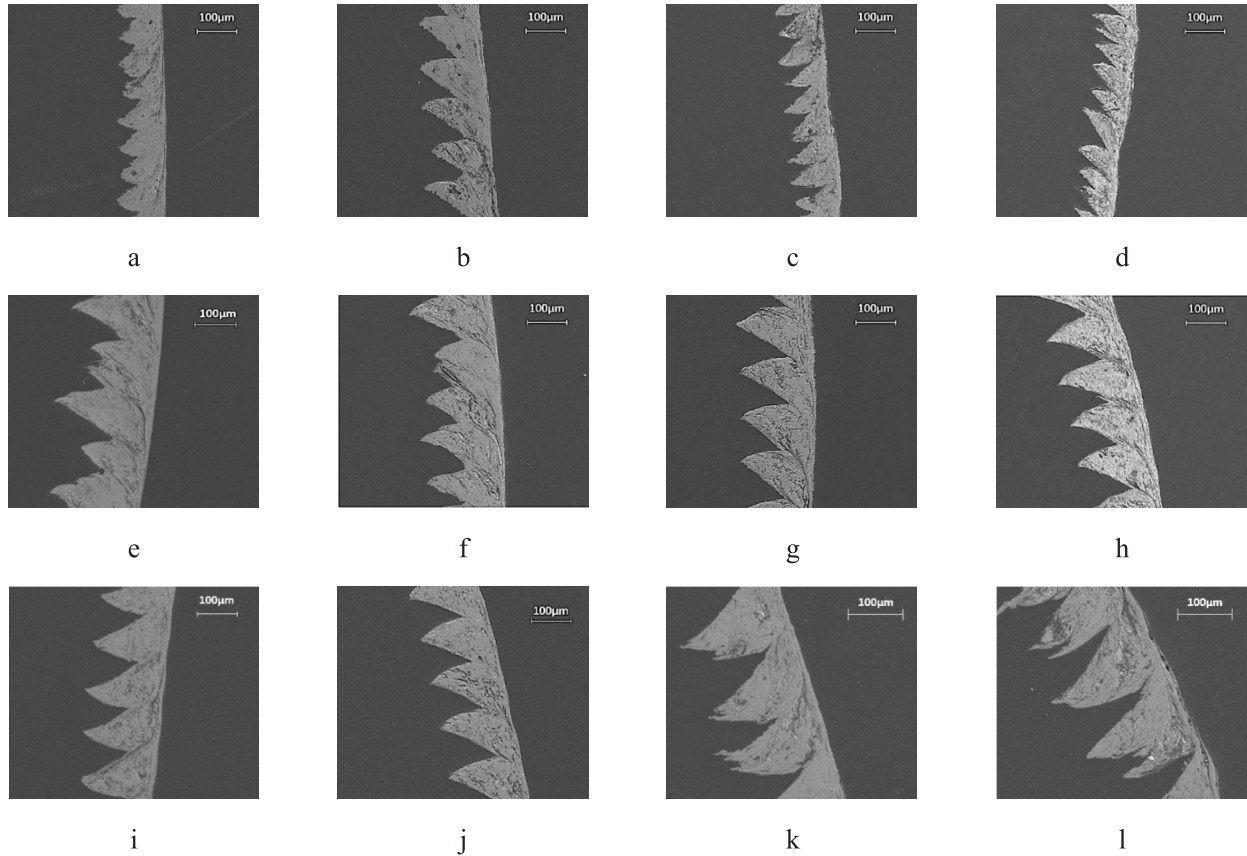

Fig. 5. SEM micrographs of the serrated chips with values of feed rate (f, mm/rev), cutting width (a_w, mm) and cutting velocity (V, m/min) of (a) $f = 0.05$, $a_w = 3.8$, $V = 50$, (b) $f = 0.05$, $a_w = 3.8$, $V = 170$, (c) $f = 0.05$, $a_w = 3.8$, $V = 300$, (d) $f = 0.05$, $a_w = 3.8$, $V = 400$, (e) $f = 0.1$, $a_w = 3.4$, $V = 50$, (f) $f = 0.1$, $a_w = 3.4$, $V = 170$, (g) $f = 0.1$, $a_w = 3.4$, $V = 300$, (h) $f = 0.1$, $a_w = 3.4$, $V = 400$, (i) $f = 0.1$, $a_w = 3.8$, $V = 300$, (j) $f = 0.1$, $a_w = 3.8$, $V = 400$, (k) $f = 0.1$, $a_w = 2.5$, $V = 300$, (l) $f = 0.1$, $a_w = 2.5$, $V = 400$.
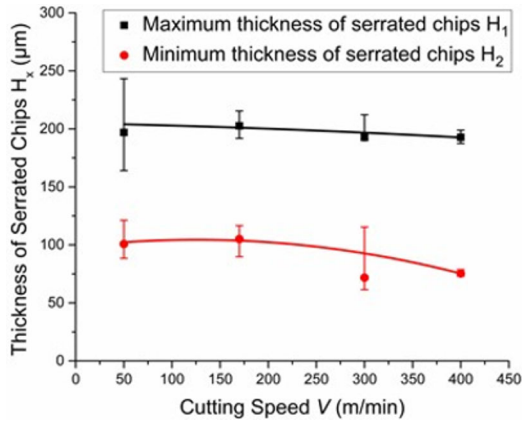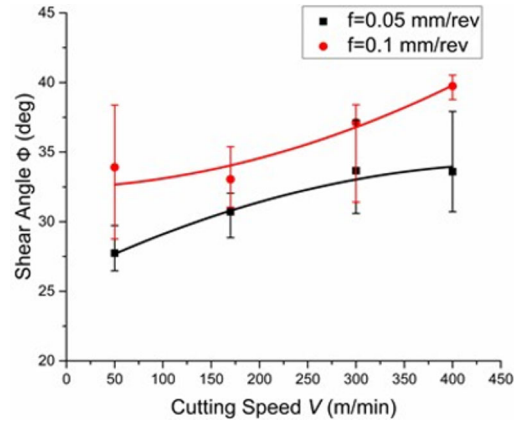
Fig. 6

Fig. 7

Fig. 6. Measured maximum and minimum chip thickness as a function of cutting speed.

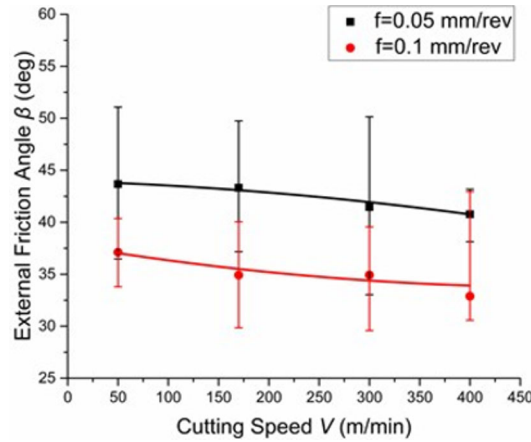Fig. 7. Calculated shear angle as a function of cutting speed.

Fig. 8. Calculated external friction angle as a function of cutting speed.

3.3. Calculation of Internal Friction Angle for Verifying Theoretical Model. The variation in the internal friction angle with different cutting settings is shown in Fig. 9. The internal friction angle of the HEA FeCoNiCrAl changes between 14.9–21.67°, which decreases slightly with increasing cutting speed, decreasing feed rate and cutting width. The internal friction angle does not change dramatically under the cutting parameters that generate serrated chips because the lubricating internal friction with softening material in the adiabatic shear band remains unchanged.

To better prove the scientificity of the new model, we cite the experimental data in the corresponding author's research results on the aluminum alloy Al6061-T6 (free cutting alloy) [20] and titanium alloy Ti-6Al-4 V (difficult-to-machine alloy) [7] as an auxiliary verification method. The size and diameter of the material are reflected in the cutting speed, and the feed is indicated in the figure. The internal friction angles of the aluminum alloy Al6061-T6 and titanium alloy Ti-6Al-4V under different cutting conditions were studied to explore the effects of material properties on the internal friction. Figure 10a shows the internal friction angle of Al6061-T6, which decreases from 42.3° to 37.4° when ribbon chips transform to serrated chips. Compared with Al6061-T6, the chips produced by cutting Ti-6Al-4V in the

cutting speed range of 20–120 m/min are all serrated with internal friction angles varying from 14.1–22.2° (Fig. 10b), and this result is very close to that of HEA FeCoNiCrAl. In summary, the internal friction angle is small when a serrated chip appears and continues to decrease as the sawtooth intensifies with increasing local temperature, dominated by the thermal conductivity and hardness of the materials. It can be inferred that, in terms of material properties, the internal friction angle is mainly affected by the thermal conductivity and hardness of the material. This inference is consistent with the material properties obtained from previous studies: the thermal conductivities of Ti-6Al-4V and HEA FeCoNiCrAl are not above 7 W/mK [30] and 23.2 W/mK [31], respectively, which are much lower than those of Al6061-T6, ranging from 162 to 253 W/m·K [32]. The hardness of Ti-6Al-4V and HEA FeCoNiCrAl are approximately HV300 and HV510, respectively, which are much higher than that of Al6061-T6's HV90. Figure 11 shows the comparison of the internal friction coefficient obtained from experiments of cutting different materials and that calculated by the classic theoretical system of shear angle.
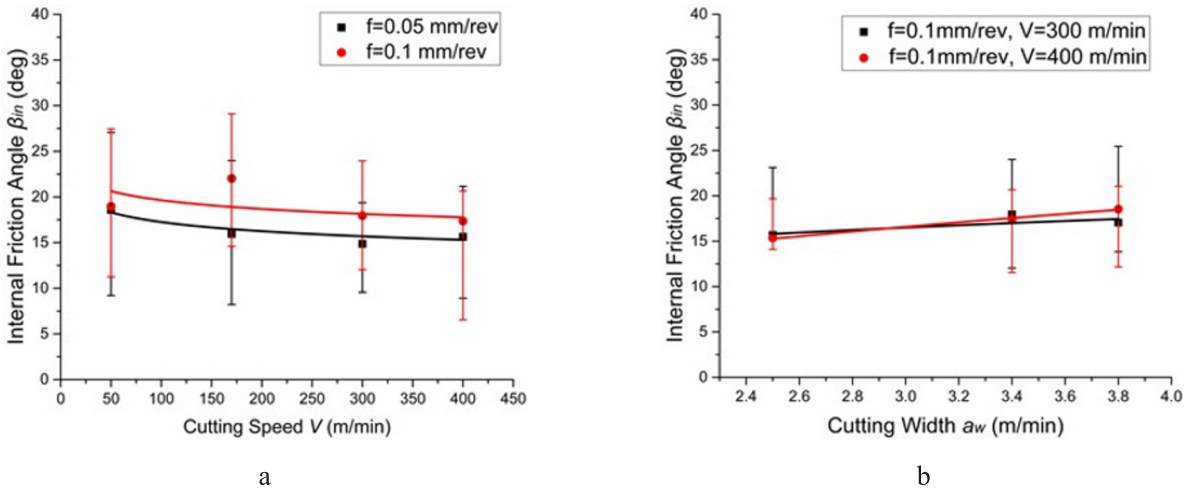

Fig. 9. Calculated internal friction angle as a function of (a) cutting speed and (b) cutting width for various feed rates.
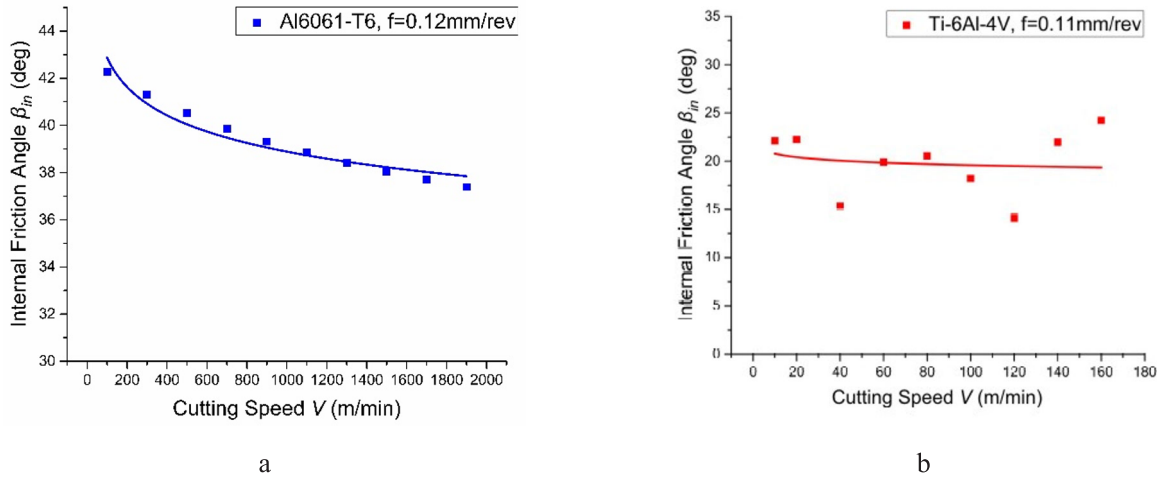

Fig. 10. Calculated internal friction angle as a function of cutting speed for (a) Al6061-T6 and (b) Ti-6Al-4V materials.

In addition, the internal friction coefficients of Al6061-T6, HEA FeCoNiCrAl and Ti-6Al-4V were calculated to obtain the applicability of the improved and traditional shear angle theories. Figure 11 shows that the internal friction coefficients of the three materials all decrease with increasing cutting speed. The internal friction coefficient of Al6061-T6 ranged from 0.909 to 0.764. This result was close to the internal friction coefficient with a value of 1, which was obtained from the Lee–Shaffer slip-line field model at low speed but gradually tended to the predictive value of von Mises when the cutting speed increased. Note that the high matching between the calculated results and classic theoretical results proves the reliability of the modified model. The internal friction angle coefficients of HEA FeCoNiCrAl and Ti-6Al-4V vary in the range of 0.265–0.395 and 0.251–0.450, respectively, which show a clear deviation from any theory of the classic theoretical system of shear angle. This is because the classic cutting theories are derived under the condition of low-speed cutting, while the internal friction coefficient values shown in Fig. 11b and (c) are obtained from high-speed cutting with serrated chips generated, and the lubrication of softening materials within the internal friction area should be considered. The adiabatic shear band between the saw teeth proves that the softened flowing material lubricates the internal friction, which leads to decreased internal friction coefficients.
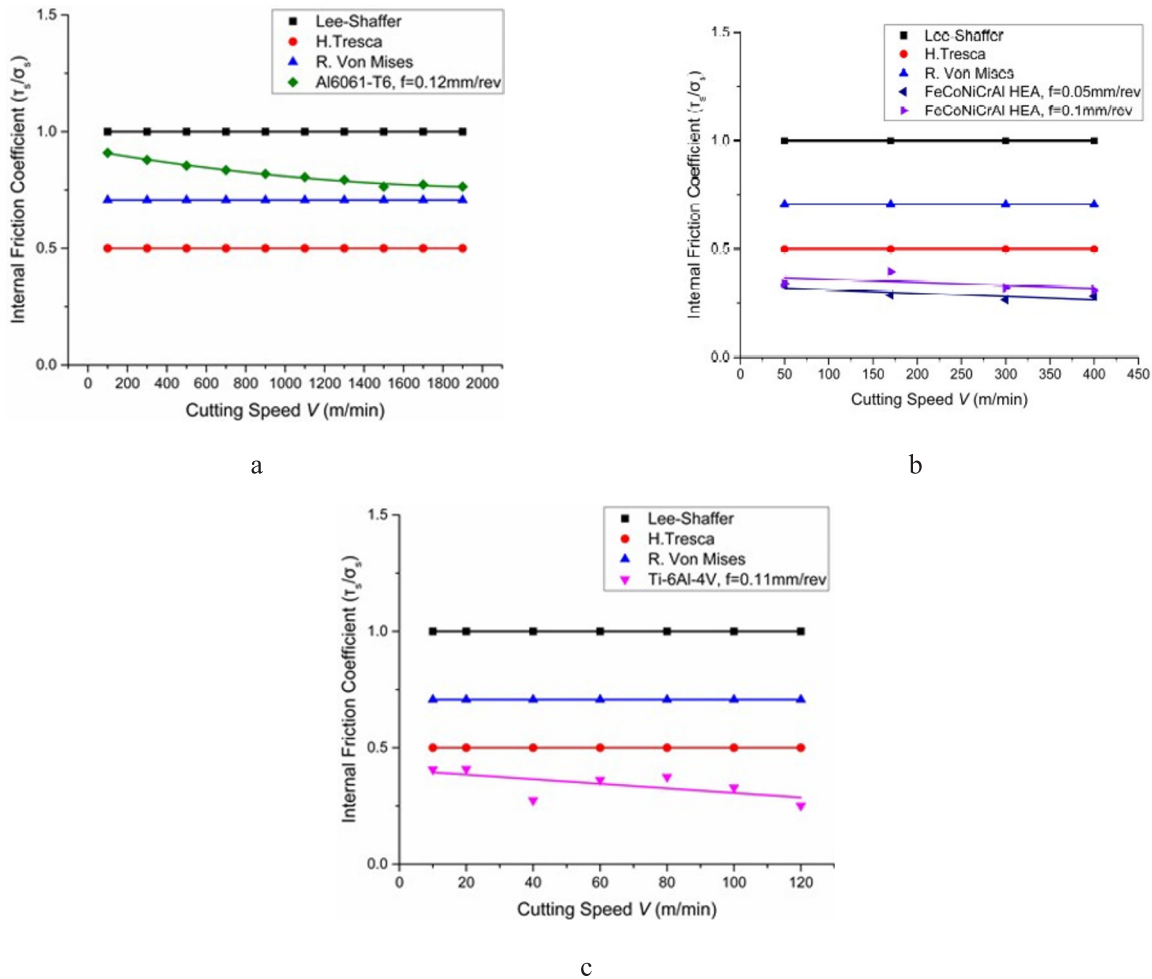

a

b

c

Fig. 11. Internal friction coefficients from (a) Al6061-T6, (b) HEA FeCoNiCrAl, (c) Ti-6Al-4V cutting experiments and classic theoretical system of shear angle.

223

Conclusions. In this study, a modified model based on conventional shear angle theories that incorporated internal friction into the forming mechanism of serrated chips and a new formula was deduced to calculate the internal friction angle. The new model formula is shown in Eq. (5). The application scope of the classic theoretical system of the shear angle, cutting characteristics of the FeCoNiCrAl HEA and change law of the internal friction angle was obtained. The main conclusions of this study are listed as follows:

1. When ribbon chips are formed in low-speed cutting, the internal friction at the slip plane is modeled well by theories proposed by Lee and Shaffer and von Mises. However, when serrated chips are formed in high-speed cutting, the modified model formula of the shear angle can better explain the mechanism of internal friction.

2. The internal friction angle varies with different cutting conditions and materials and is prone to decline with a high local cutting temperature, which is dominated by the high cutting speed and low thermal conductivity of materials.

3. The cutting experiment results herein indicated that the cutting settings of the HEA FeCoNiCrAl should include a large cutting speed, small feed rate and small cutting width. These settings can mitigate the cutting force, prolong the tool life and lower the cost when rough processing this HEA.

REFERENCES

1. J. W. Yeh, S. K. Chen, S. J. Lin, et al., "Nanostructured high-entropy alloys with multiple principal elements: novel alloy design concepts and outcomes," *Adv Eng Mater*, **6**, No. 5, 299–303 (2004).
2. D. B. Miracle and O. N. Senkov, "A critical review of high entropy alloys and related concepts," *Acta Mater*, **122**, 448–511 (2017).
3. B. E. MacDonald, Z. Fu, B. Zheng, et al., "Recent progress in high entropy alloy research," *JOM*, **69,** No. 10, 2024–2031 (2017).
4. W. R. Wang, W. L, Wang, S. C. Wang, et al., "Effects of Al addition on the microstructure and mechanical property of AlxCoCrFeNi high-entropy alloys," *Intermetallics,* **26,** 44–51 (2012).
5. E. J. Pickering and N. G. Jones, "High-entropy alloys: a critical assessment of their founding principles and future prospects," *Int Mater Rev,* **61**, No. 3, 183–202 (2016).
6. J. Y. He, H. Wang, H. L. Huang, et al., "A precipitation-hardened high-entropy alloy with outstanding tensile properties," *Acta Mater*, **102**, 187–196 (2016).
7. W. X. Li, D. C. Xu, D. P. Xiong, et al., "Compression deformation in the primary zone during the high-speed cutting of titanium alloy Ti-6Al-4V," *Int J Adv Manuf Tech*, **102**, No. 9, 4409–4417 (2019).
8. Y. S. Su, L. Li, G. Wang, et al., "Cutting mechanism and performance of high-speed machining of a titanium alloy using a super-hard textured tool," *J Manuf Process*, **34**, 706–712 (2018).
9. R. Komanduri and Z. B. Hou, "On thermoplastic shear instability in the machining of a titanium alloy (Ti-6Al-4V)," *Metall Mater Trans A*, **33**, No. 9, 2995–3010 (2002).
10. Q. B. Yang, Y. Wu, D. Liu, et al., "Characteristics of serrated chip formation in high-speed machining of metallic materials," *Int J Adv Manuf Tech*, **86**, No. 5, 1201–1206 (2016).
11. Q. C. Ke, D. C. Xu, and D. P. Xiong, "Cutting zone area and chip morphology in high-speed cutting of titanium alloy Ti-6Al-4V," *J Mech Sci Technol*, **31**, No. 1, 309–316 (2017).

12. D. C. Xu, P. F. Xu, W. B. Li, et al., "Research on chip formation parameters of aluminum alloy 6061-T6 based on high-speed orthogonal cutting model," *Int J Adv Manuf Tech*, **72**, No. 5, 955–962 (2014).

13. X. L. Fu, B. Zhou, Y. Meng, et al., "Study on the constitutive model of anisotropic aluminum alloy in high speed cutting," *Mach Sci Technol*, **24**, No. 6, 906–923 (2020).

14. I. Ullah, S. Zhang, Q. Zhang, et al., "Numerical investigation on serrated chip formation during high-speed milling of Ti-6Al-4V alloy," *J Manuf Process*, **71**, 589–603 (2021).

15. W. Jomaa, O. Mechri, J. Lévesque, et al., "Finite element simulation and analysis of serrated chip formation during high-speed machining of AA7075–T651 alloy," *J Manuf Process*, **26**, 446–458 (2017).

16. B. Wang, Z. Q. Liu, X. Hou, et al., "Influences of cutting speed and material mechanical properties on chip deformation and fracture during high-speed cutting of Inconel 718," *Materials*, **11**, No. 4, 461 (2018).

17. C. Zhang and H. Choi, "Study of segmented chip formation in cutting of high-strength lightweight alloys," *Int J Adv Manuf Tech*, **112**, No. 9, 2683–2703 (2021).

18. S. Atlati, A. Moufki, M. Nouari, et al., "Interaction between the local tribological conditions at the tool–chip interface and the thermomechanical process in the primary shear zone when dry machining the aluminum alloy AA2024–T351," *Tribol Int*, **105**, 326–333 (2017).

19. S. Bahi, G. List, and G. Sutter, "Modeling of friction along the tool-chip interface in Ti6Al4V alloy cutting," *Int J Adv Manuf Tech*, **84**, No. 9, 1821–1839 (2016).

20. M. H. Hao, D. C. Xu, F. Q. Wei, et al., "Quantitative analysis of frictional behavior of cupronickel B10 at the tool-chip interface during dry cutting," *Tribol Int*, **118**, 163–169 (2018).

21. C. Y. Zhang, J. P. Lu, F P. Zhang, et al., "Identification of a new friction model at tool-chip interface in dry orthogonal cutting," *Int J Adv Manuf Tech*, **89**, No. 1, 921–932 (2017).

22. L. Q. Tu, W. W. Ming, X. W. Xu, et al., "Wear and failure mechanisms of SiAlON ceramic tools during high-speed turning of nickel-based superalloys," *Wear*, **488**, 204171 (2022).

23. C. Z. Duan, W. Sun, C. Fu, et al., "Modeling and simulation of tool-chip interface friction in cutting Al/SiCp composites based on a three-phase friction model," *Int J Mech Sci*, **142**, 384–396 (2018).

24. M. E. Merchan, "Mechanics of the metal cutting process I," *J Appl Phys*, **16**, 267–318 (1945).

25. E. H. Lee and B. W. Shaffer, "The theory of plasticity applied to a problem of machining," *J Appl Mech*, **18**, No. 4, 405–413 (1951).

26. Y. Altintas, *Manufacturing Automation: Metal Cutting Mechanics, Machine Tool Vibrations, and CNC Design*, 2nd edn, Cambridge University Press (2012).

27. M. C. Shaw and J. O. Cookson, *Metal Cutting Principles*, Vol. 2, Oxford University Press, New York (2005).

28. S. J. Zhang, P. Guo, Z. W. Xiong, et al., "Cyclic shear angle for lamellar chip formation in ultra-precision machining," *P I Mech Eng C-J. Mec*, **234**, No. 13, 2673–2680 (2020).

29. S. C. Sui and P. F. Feng, "Investigation of serrated chip morphology change regular in the burning of titanium alloys," *Int J Adv Manuf Tech*, **87**, No. 9, 2665–2671 (2016).

30. F. Z. Wang, K. X. Ji, and Z. Y. Guo, "Microstructural analysis of failure progression for coated carbide tools during high-speed milling of Ti-6Al-4V," *Wear*, **456**, 203356 (2020).

31. M. N. Zhang, *Microstructure and Properties of CoCrMoNbTi and AlCoCuFeNi High Entropy Alloys by Additive Manufacturing Technology* [in Chinese], PhD Thesis, University of Science and Technology, Beijing (2018).

32. B. G. Kıral, M. Tabanoğlu, and H. T. Serindağ, "Finite element modeling of friction stir welding in aluminum alloys joint," *Math Comput Appl*, **18**, No. 2, 122–131 (2013).